Supporting Information for:

Multifunctional Applications of Blow Spinning *Setaria viridis* Structured Fibrous Membranes in Water Purification

Tao Lu[1], Yankang Deng[1], Jiaxin Cui[1], Wenxuan Cao[1], Qingli Qu[1], Yulin Wang[1], Ranhua Xiong[1], Wenjing Ma[1*], Jiandu Lei[2*], Chaobo Huang[1*]

1. Joint Laboratory of Advanced Biomedical Materials (NFU-UGent), Jiangsu Co-Innovation Center of Efficient Processing and Utilization of Forest Resources, Nanjing Forestry University, Nanjing, 210037, P. R. China
2. Beijing Key Laboratory of Lignocellulosic Chemistry, and MOE Engineering Research Center of Forestry Biomass Materials and Bioenergy, Beijing Forestry University, Beijing, 100083, P. R. China

*E-mail: mawenjing@njfu.edu.cn (Wenjing Ma)

*E-mail: ljd2012@bjfu.edu.cn (Jiandu Lei)

*E-mail: chaobo.huang@njfu.edu.cn (Chaobo Huang)

S1 Methods and materials

1.1. Mechanism of core-shell needle for blow-spinning

Blow-spinning is another way to prepare nanofibers, which requires two parallel coaxial needles. The inner layer is filled with polymer solution, and the outer layer is filled with pressurized gas flow, so that the fibers are deposited along the gas flow direction. In general, the air flow spinning equipment is composed of air flow source, liquid injection pump, spinning needle and collecting device. The basic principle is that under the high-speed air flow, the spinning liquid flow is rapidly stretched and refined to obtain nanofibers.[1]

There are many factors that affect the blow-spinning process, such as polymer concentration, molecular weight, air flow speed, receiving distance, liquid injection speed, ambient temperature and humidity. Compared with the existing preparation methods of nanofibers, blow-spinning has the advantages of wide applicability of raw materials, small fiber diameter under the same shear force and low energy

consumption. And the spinning equipment is simple, low cost, flexible operation. Compared with electrospinning, blow-spinning does not need high pressure, so the preparation process is safer, the production efficiency is higher, and the collection device is easier to choose.

1.2. Preparation of oil/water mixture and oil-in-water emulsions

The oil/water mixture was prepared by mixing oils and water (1/1, V/V).[2] For the surfactant-free oil-in-water emulsions (SFE),[3] the oils and water were mixed in a volume ratio of 1:9, and the mixtures were under ultrasonic treatment for 2 h at 25-30 °C to obtain the emulsified, milky solutions. To prepare the surfactant-stabilized oil-in-water emulsions (SSE),[3] the Span 80 was first dissolved in water as the emulsifier, then the related oil was added to water, and the volume ratio of the oil and water was fixed to 1:99. Then, the mixtures were under ultrasonic treatment for 1 h at 25-30 °C to produce a milky emulsion. The as-prepared surfactant-stabilized oil-in-water emulsions could be stable for at least 24 h.

1.3. Oil/water mixtures and oil-in-water emulsion separation experiments

The oil/water separation performance was evaluated using a home-made filtrated apparatus. The membranes were fixed between two vertical glass tubes with an inner diameter of ≈ 15 mm. The mixtures or emulsions were directly poured onto the membrane, and the water spontaneously permeated. It was noted that the separation was driven by the gravity of the solutions. The permeation flux was determined by calculating the quantity of the permeate per unit time based on previous studies.[4] The separation efficiency was assessed by measuring the total organic carbon contents of the feed solutions and the corresponding filtrate. The flux (F, $L \cdot m^{-2}\ h^{-1}$) was determined by the volume of filtrates per unit time according to the equation:

$$F = \frac{V}{A\,\Delta t} \quad (1)$$

where V (L) is the oil volume in the mixture, A (m^2) is the area of the nanofibrous membrane exposed to the oil-water mixture, and Δt (h) is the time required for complete permeation of water.

The separation efficiency (η), the mass ratio of water before and after separation, was

calculated according to the following equation:

$$\eta = (\frac{m_1}{m_0}) \times 100 \quad (2)$$

where m_0 is the weight of the water before separation, and m_1 is the weight of the water after separation.

1.4. Evaluation of the photocatalytic activity

The photocatalytic activity of the membrane was studied according to the reported method.[5] The degradation of Methyl orange (MO) was used to evaluate the photocatalytic performance of ZnO/PANI/PAN nanofibrous composite membrane.[6] The whole degradation process was carried out in a 100 mL glass device with recycled water to maintain the room temperature. A 300 W xenon lamp with a 350-780 nm optical filter (CEL-HXF300) was used as a typical visible-light source. The distance from the lamp to the reaction liquid was 10 cm. Typically, the as-fabricated membranes (0.1 g) were added into 50 mL of MO solution (10 ppm) and stirred at 200 rpm for 60 min in the dark to reach the adsorption equilibrium. After a fixed time interval, 2 mL of dyes from solutions was taken out to monitor the concentration of remnant dyes by a UV-vis spectrophotometer. The degradation rate (η %) was defined as:

$$\eta = \frac{A_0 - A_t}{A_0} \quad (3)$$

where A_0 is the absorbance in 469 nm wavelength of raw solution, and A_t is the absorbance in 469 nm wavelength of solution at every time, used because 469 nm is the characteristic wavelength of MO aqueous solution in visible light.

1.5. Antibacterial activity testing

The antibacterial activity testing was carried out according to our previous work.[7] Bacillus subtilis (*B. sub*, Gram-positive) and Escherichia coli (*E. coli*, Gram-negative) were used for the antibacterial test. Briefly, *B. sub* and *E. coli* were pre-cultured and diluted with nutrient broth to obtain a test inoculum. Agar solution was poured into a disposable sterile culture dish (diameter of 90 mm) and allowed to solidify. Then, 0.3 mL of the test inoculum was uniformly distributed onto the agar plate surface, respectively, on which the as-prepared electrospun nanofibrous membranes with a

diameter of 8 mm were placed after ultraviolet sterilization. Then the culture dishes were incubated for 24 h at 37 °C. The antimicrobial activity of the membranes was evaluated by measuring the radius of the bacterial diffusion inhibition zone.

1.6. Biosafety

Zebrafish has been widely used in basic research of life science, chemical safety and environmental toxicology monitoring.[8-10] The Biosafety of the membrane was studied according to the reported method.[11] Therefore, in this study, Zebrafish (Danio rerio, Mean length ≈ 1-1.5cm) were purchased from Lekai Co., Ltd. (Shanghai, China) as the in vivo model to assess the toxicity of ZnO/PANI/PAN membranes under visible light. Briefly, zebrafish were domesticated under laboratory conditions (a temperature of 27 ± 1 °C and a photoperiod of 12:12 h (L/D)) for more than 7 days before the experiment, and mortality was kept below 5%. Zebrafish were fed 1 time a day with commercially available bait, and food residues were removed promptly. Feeding was stopped 24 h before the start of the formal experiment. After, zebrafish were cultured in two Petri dishes, one was added with 1.5g ZnO/PANI/PAN membranes (about 10 pieces of 2×2 cm membranes), the other was as control, and the survival of zebrafish was recorded at 5, 10 and 15 d, respectively.

S2 Figures

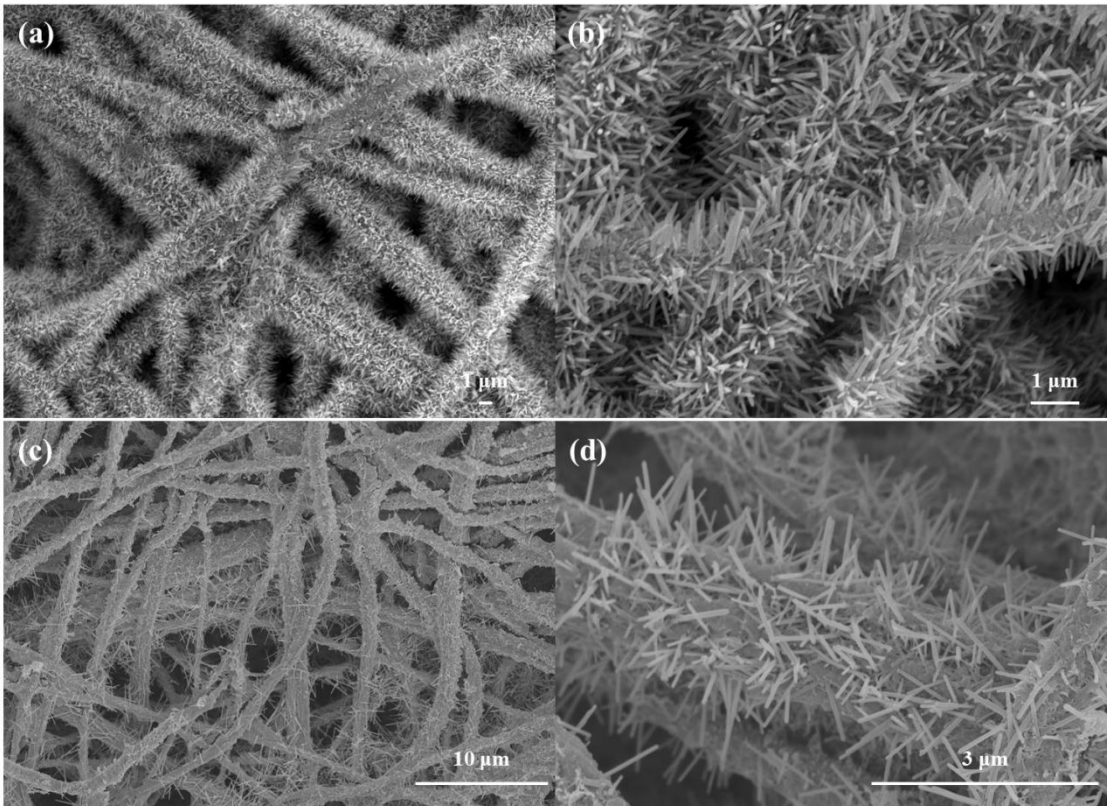

Figure S1. SEM images of ZnO/PANI/PAN fibrous membranes with different $Zn(NO_3)_2 \cdot 6H_2O$ contents. (a) 26 mg/mL; (c) 13 mg/mL; (b) and (d) were the corresponding high-magnification images of the previous two respectively.

The SEM images showed the effect of the $Zn(NO_3)_2 \cdot 6H_2O$ concentration on the morphology of the fibers. When the concentration of $Zn(NO_3)_2 \cdot 6H_2O$ was 26 mg/mL, the results showed that more ZnO nanoneedles are grown on the surface of the fiber. However, when the concentration was reduced to 13 mg/mL, the density of nanosized ZnO on the fiber surface decreased obviously.

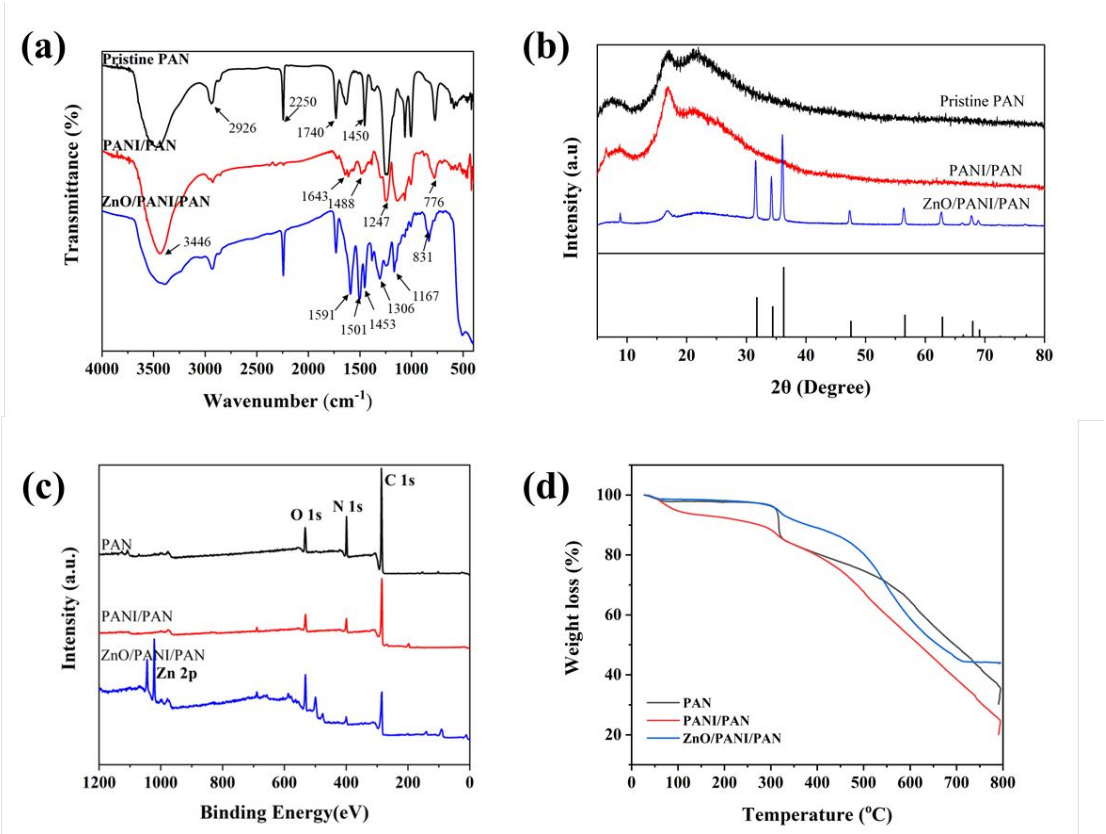

Figure S2. (a) FTIR spectra, (c) XRD peaks, (c) XPS spectra and (d) TG curve of PAN, PANI/PAN and ZnO/PANI/PAN.

The FTIR spectra of the membranes were investigated in Fig. S1a to verify the success of the preparation of multifunctional ZnO/PANI/PAN composite membrane. It can be seen that the absorption vibration peak at 2250 cm^{-1} belongs to the stretching vibration peak of cyano (-CN).[12] The vibration peaks at 1643 and 1488 cm^{-1} are the stretching vibration peaks of quinone structure and benzene structure in PANI, and the vibration peaks at 1247 cm^{-1} are the stretching vibration peaks of C-N in aromatic amine. The bending vibration peaks of C-H are located at 1138 cm^{-1} and 776 cm^{-1}, which are characteristic peaks of PANI conductivity and electron delocalization. The above characteristic peaks of PANI indicate the existence of PANI, and these peaks still exist after the growth of ZnO, indicating that the hydrothermal reaction process has no effect on the molecular structure of PANI. However, after the growth of ZnO, a small shift was observed in the characteristic peaks of PANI, the vibration peaks at 1643 cm^{-1} and 1488 cm^{-1} shifted to 1731 cm^{-1} and 1591 cm^{-1}, respectively; the

vibration peaks at 1138 cm^{-1} and 776 cm^{-1} shifted to 1167 cm^{-1} and 831 cm^{-1}, respectively. This phenomenon may be due to the strong electrostatic interaction between ZnO and PANI.[13-14] Fig. S1b shows the XRD patterns of PAN, PANI/PAN and ZnO/PANI/PAN composite fibrous membranes. Compared with the standard spectrum (JCPDS36-1451), it is proved that the diffraction of the sample is mainly attributed to wurtzite structure ZnO.[15-16] This indicates that ZnO nanorods are successfully deposited on the fiber surface. The surface chemical composition of membranes was further investigated by X-ray photoelectron spectroscopy (XPS). As displayed in Fig. S1c, the XPS survey spectra indicates that the pure PAN sample was composed of the elements C and N. The presence of the strong Zn 2p and O 1s peaks, together with the attenuation of N1s peak, confirmed that the ZnO had been grown successfully onto the membrane surface. In order to quantitatively study the proportion of each component in ZnO/PANI/PAN composite nanofibers, the samples were tested by thermogravimetry. Each sample was heated from room temperature to 800 ^{o}C at a rate of 10 ^{o}C/min. Finally, the thermal decomposition diagrams of PAN、PANI/PAN and ZnO/PANI/PAN composite fibrous membranes were obtained, as shown in Fig. S1d. In order to study the proportion of each component in ZnO/PANI/PAN composite nanofibers, the samples were tested by thermogravimetry. Each sample was heated from room temperature to 800^{o}C at a rate of 10 ^{o}C/min. Finally, their thermal decomposition diagram is obtained, as shown in Fig. S2d. It can be seen from the figure that the organic polymer decomposes after high temperature heating, and only the ZnO remained, indicating that the ZnO loading in the sample is 44.2%.

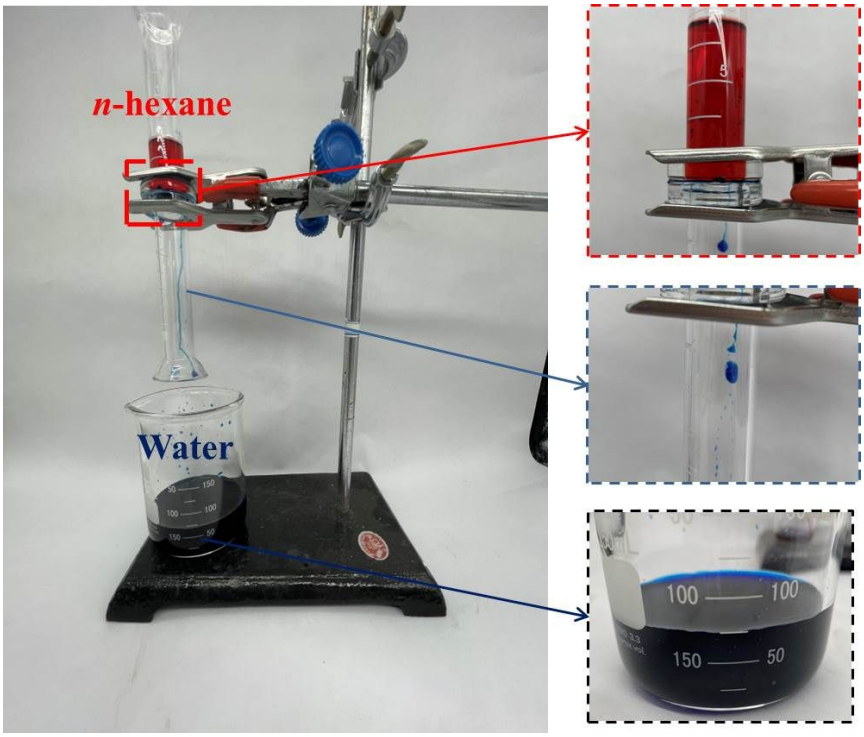

Figure S3. The separation process for *n*-hexane/water mixture.

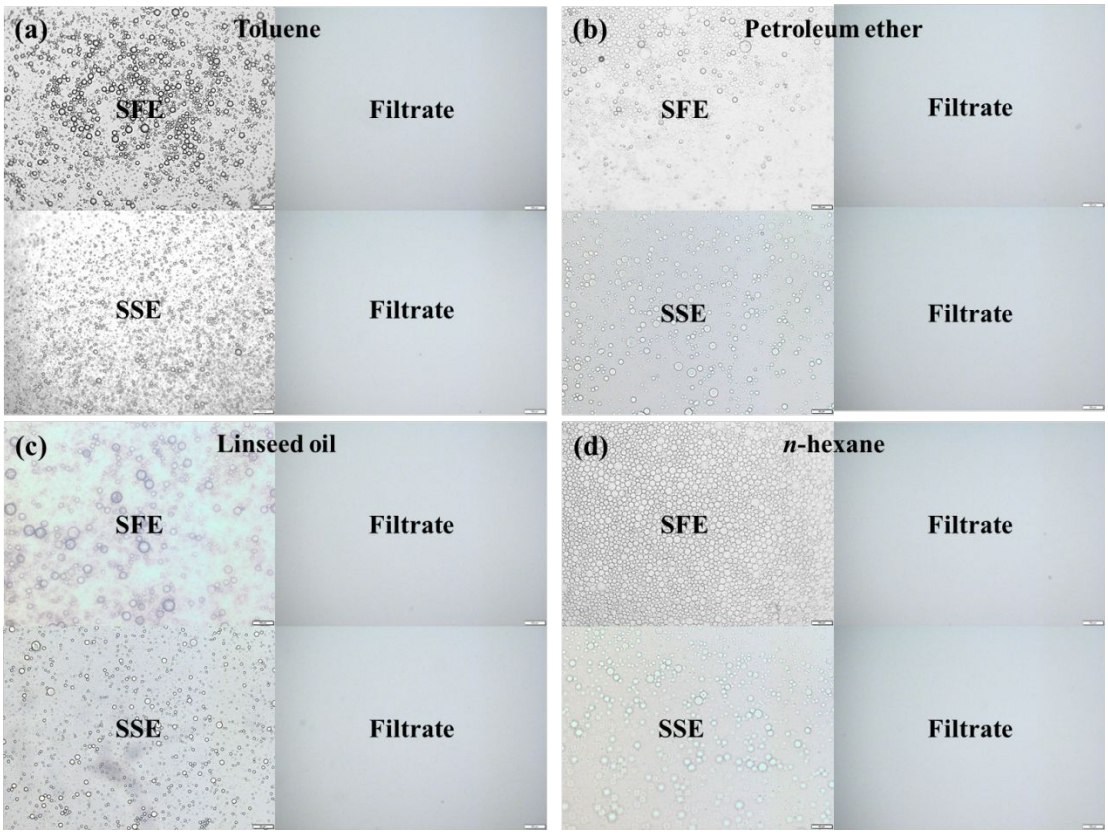

Figure S4. Optical microscopy images of the (a) toluene-in-water, (b) petroleum ether-in-water, (c) linseed oil-in-water and (d) *n*-hexane-in-water SFE and SSE before

and after filtration

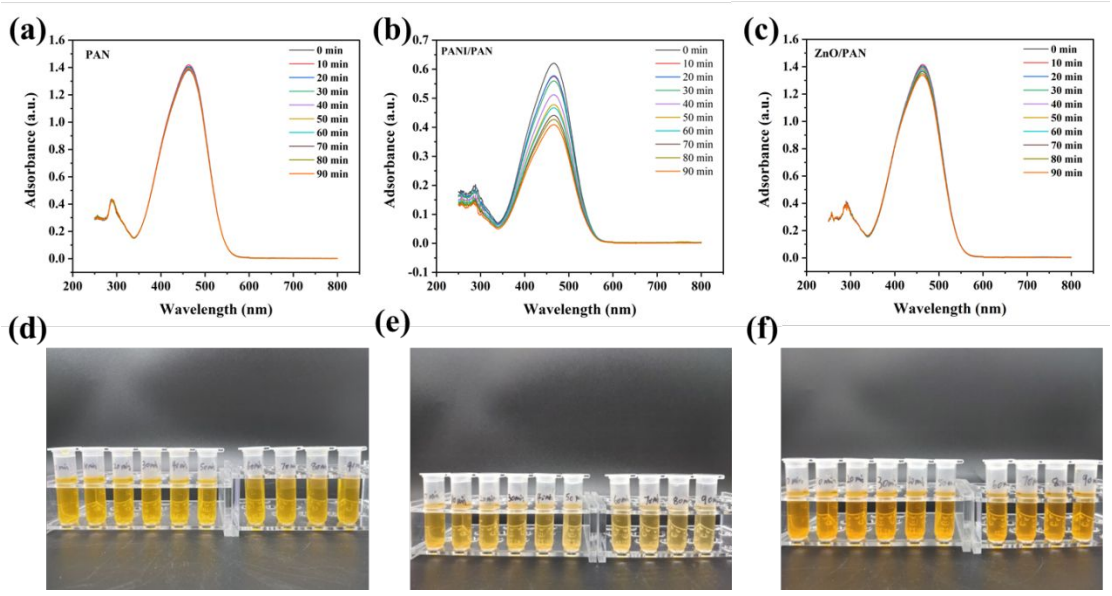

Figure S5. UV-vis absorption spectra of the MO dye as a function of sunlight irradiation time for (a) MO dye solution mixed with PAN nanofibrous membrane, (b) PANI/PAN nanofibrous membrane and (c) ZnO/PAN nanofibrous membrane.

Table S1. Comparison of the permeate fluxes (L m^{-2} h^{-1}) and separation efficiencies (%) of various emulsions using the nanofibrous membranes

Materials	Emulsions	Surfactants	Permeate fluxes (L m^{-2} h^{-1})	Separation efficiency (%)	Ref.
ZnO/PANI/PAN membrane	O/W (10 vol%) Toluene, *n*-hexane, kerosene, petroleum ether, linseed oil	Span 80	2253.50	> 99	This work
PP/WO3/PAN membrane	O/W (10 vol%) N-hexane, petroleum ether, toluene, kerosene, soybean oil	Tween 80	671	> 99	2
MOF-808-PAN membrane	O/W (10 vol%) N-hexane, gasoline, soybean oil	SDS, CTAB, Tween 20	379.3	> 99.97	17
Loess-coated PVDF membrane	O/W (2 vol%) Kerosene, Diesel, heptane, *n*-hexane, petroleum ether and crude oil	Tween 80	423	> 99.2	18
Amino-Functionalized porous nanofibrous membrane	O/W (1 vol%) Cyclohexane, *n*-hexane, petroleum ether, tetradecane, ethane dichloride	CTAB	622	99.26	19

PAA-g-PVDF filtration membrane	O/W (1 vol%) Hexadecane, toluene, diesel,	SDS, Tween 80,	570	99.99	20
ZIF-8/PAN membrane	O/W (2 vol%) Crude oil, motor oil, DCM, DCE and chloroform	SDS	2514	99	21
CNC, ChiNC and CS coating PET nonwoven	W/O (8 vol%) Corn oil	SDS	597	99.2	22
PFDT/PDA/PI membranes	W/O (2 vol%) Toluene, hexane, chloro-form and kerosene	Span 80	—	99	23
Wood membrane	W/O (1 vol%) *N*-octane, toluene	SDS	460.8	99.43	24
HDT-Ag-PDA-Al2O3 membrane	W/O (0.5 vol%) Octane	Span 80	1915	98.6	25
FG@PDA@PDMS membrane	W/O (1 vol%) Toluene	Span 80	734	98.4	26
PVC/SiO_2 membrane	W/O (1 vol%) Toluene, kerosene	Span 80	358.6	95	27

Notes: "—" means that the corresponding parameters are not mentioned in the article.

REFERENCES

(1) Daristotle, J. L.; Behrens, A. M.; Sandler, A. D.; Kofinas, P. A Review of the Fundamental Principles and Applications of Solution Blow Spinning. *ACS Appl. Mater. Interfaces* **2016,** *8* (51), 34951-34963.

(2) Ma, W.; Li, Y.; Gao, S.; Cui, J.; Qu, Q.; Wang, Y.; Huang, C.; Fu, G. Self-Healing and Superwettable Nanofibrous Membranes with Excellent Stability toward Multifunctional Applications in Water Purification. *ACS Appl. Mater. Interfaces* **2020,** *12* (20), 23644-23654.

(3) Ge, J.; Jin, Q.; Zong, D.; Yu, J.; Ding, B. Biomimetic Multilayer Nanofibrous Membranes with Elaborated Superwettability for Effective Purification of Emulsified Oily Wastewater. *ACS Appl. Mater. Interfaces* **2018,** *10* (18), 16183-16192.

(4) Ma, W.; Zhang, M.; Liu, Z.; Kang, M.; Huang, C.; Fu, G. Fabrication of Highly Durable and Robust Superhydrophobic-Superoleophilic Nanofibrous Membranes Based on a Fluorine-free System for Efficient Oil/Water Separation. *J. Membr. Sci.* **2019,** *570-571*, 303-313.

(5) Ahmed, B.; Ojha, A. K.; Singh, A.; Hirsch, F.; Fischer, I.; Patrice, D.; Materny, A. Well-Controlled In-situ Growth of 2D WO_3 Rectangular Sheets on Reduced Graphene Oxide with Strong Photocatalytic and Antibacterial Properties. *J. Hazard. Mater.* **2018,** *347*, 266-278.

(6) Chang, J. S.; Strunk, J.; Chong, M. N.; Poh, P. E.; Ocon, J. D., Multi-Dimensional Zinc Oxide (ZnO) Nanoarchitectures as Efficient Photocatalysts: What is the Fundamental Factor that Determines Photoactivity in ZnO? *J. Hazard. Mater.* **2020,** *381*, 120958.

(7) Ma, W.; Ding, Y.; Zhang, M.; Gao, S.; Li, Y.; Huang, C.; Fu, G. Nature-Inspired Chemistry toward Hierarchical Superhydrophobic, Antibacterial and Biocompatible Nanofibrous Membranes for Effective UV-Shielding, Self-cleaning and Oil-Water Separation. *J. Hazard. Mater.* **2020,** *384*, 121476.

(8) Ren, C.; Hu, X.; Li, X.; Zhou, Q. Ultra-Trace Graphene Oxide in a Water Environment Triggers Parkinson's Disease-like Symptoms and Metabolic Disturbance in Zebrafish Larvae. *Biomaterials* **2016,** *93*, 83-94.

(9) Amanuma, K.; Takeda, H.; Amanuma, H.; Aoki, Y. Transgenic Zebrafish for Detecting Mutations Caused by Compounds in Aquatic Environments. *Nat. Biotechnol.* **2000,** *18* (1), 62-65.

(10) Garcia, G. R.; Noyes, P. D.; Tanguay, R. L. Advancements in Zebrafish Applications for 21st Century Toxicology. *Pharmacol. Ther.* **2016,** *161*, 11-21.

(11) Zhang, L.; Ren, S.; Chen, C.; Wang, D.; Liu, B.; Cai, D.; Wu, Z. Near Infrared Light-Driven Release of Pesticide with Magnetic Collectability using Gel-Based Nanocomposite. *Chem. Eng. J.* **2020**, 127881.

(12) Emani, P. S.; Maddah, H. A.; Rangoonwala, A.; Che, S.; Prajapati, A.; Singh, M. R.; Gruen, D. M.; Berry, V.; Behura, S. K. Organophilicity of Graphene Oxide for Enhanced Wettability of ZnO Nanorods. *ACS Appl. Mater. Interfaces* **2020,** *12* (35), 39772-39780.

(13) Ou, B.; Wang, J.; Wu, Y.; Zhao, S.; Wang, Z. Reuse of PANI Wastewater Treated by Anodic Oxidation/Electro-Fenton for the Preparation of PANI.

Chemosphere **2020,** *245*, 125689.
(14) Saravanan, R.; Sacari, E.; Gracia, F.; Khan, M. M.; Mosquera, E.; Gupta, V. K. Conducting PANI Stimulated ZnO System for Visible Light Photocatalytic Degradation of Coloured Dyes. *J. Mol. Liq.* **2016,** *221*, 1029-1033.
(15) Pan, T.; Liu, J.; Deng, N.; Li, Z.; Wang, L.; Xia, Z.; Fan, J.; Liu, Y., ZnO Nanowires@PVDF Nanofiber Membrane with Superhydrophobicity for Enhanced Anti-Wetting and Anti-Scaling Properties in Membrane Distillation. *J. Membr. Sci.* **2021,** *621*, 118877.
(16) Huang, Q.-L.; Huang, Y.; Xiao, C.-F.; You, Y.-W.; Zhang, C.-X. Electrospun Ultrafine Fibrous PTFE-Supported ZnO Porous Membrane with Self-Cleaning Function for Vacuum Membrane Distillation. *J. Membr. Sci.* **2017,** *534*, 73-82.
(17) Chen, X.; Chen, D.; Li, N.; Xu, Q.; Li, H.; He, J.; Lu, J. Modified-MOF-808-Loaded Polyacrylonitrile Membrane for Highly Efficient, Simultaneous Emulsions Separation and Heavy Metal Ions Removal. *ACS Appl. Mater. Interfaces* **2020**, 12, 35, 39227-39235.
(18) Wang, X.; Li, M.; Shen, Y.; Yang, Y.; Feng, H.; Li, J. Facile Preparation of Loess-coated Membranes for Multifunctional Surfactant-Stabilized Oil-in-Water Emulsion Separation. *Green Chem.* **2019,** *21* (11), 3190-3199.
(19) Wang, Y.; Wang, B.; Wang, Q.; Di, J.; Miao, S.; Yu, J. Amino-Functionalized Porous Nanofibrous Membranes for Simultaneous Removal of Oil and Heavy-Metal Ions from Wastewater. *ACS Appl. Mater. Interfaces* **2019,** *11* (1), 1672-1679.
(20) Zhang, W.; Zhu, Y.; Liu, X.; Wang, D.; Li, J.; Jiang, L.; Jin, J. Salt-Induced Fabrication of Superhydrophilic and Underwater Superoleophobic PAA-g-PVDF Membranes for Effective Separation of Oil-in-Water Emulsions. *Angew Chem., Int. Ed. Engl.* **2014,** *53* (3), 856-860.
(21) Li, H.; Mu, P.; Li, J.; Wang, Q. Inverse Desert Beetle-like ZIF-8/PAN Composite Nanofibrous Membrane for Highly Efficient Separation of Oil-in-Water Emulsions. *J. Mater. Chem. A* **2021,** *9* (7), 4167-4175.
(22) Yagoub, H.; Zhu, L.; Shibraen, M. H. M. A.; Altam, A. A.; Babiker, D. M. D.; Rehan, K.; Mukwaya, V.; Xu, J.; Yang, S. Manipulating the Surface Wettability of Polysaccharide Based Complex Membrane for Oil/Water Separation. *Carbohydr. Polym.* **2019,** *225*, 115231.
(23) Ma, W.; Zhao, J.; Oderinde, O.; Han, J.; Liu, Z.; Gao, B.; Xiong, R.; Zhang, Q.; Jiang, S.; Huang, C. Durable Superhydrophobic and Superoleophilic Electrospun Nanofibrous Membrane for Oil-Water Emulsion Separation. *J. Colloid Interface Sci.* **2018,** *532*, 12-23.
(24) Kim, S.; Kim, K.; Jun, G.; Hwang, W. Wood-Nanotechnology-Based Membrane for the Efficient Purification of Oil-in-Water Emulsions. *ACS Nano* **2020**, 14, 12, 17233-17240.
(25) Gao, N.; Xu, Z.-K. Ceramic Membranes with Mussel-Inspired and Nanostructured Coatings for Water-in-Oil Emulsions Separation. *Sep. Purif. Technol.* **2019,** *212*, 737-746.
(26) Kang, H.; Zhang, X.; Li, L.; Zhao, B.; Ma, F.; Zhang, J., Polydopamine and Poly(dimethylsiloxane) Modified Superhydrophobic Fiberglass Membranes for

Efficient Water-in-Oil Emulsions Separation. *J. Colloid Interface Sci.* **2020,** *559*, 178-185.
(27) Xu, H.; Liu, H.; Huang, Y.; Xiao, C., Three-Dimensional Structure Design of Tubular Polyvinyl Chloride Hybrid Nanofiber Membranes for Water-in-Oil Emulsion Separation. *J. Membr. Sci.* **2021,** *620*, 118905.